Time exposure performance of Mo–Au Gibbsian segregating alloys for extreme ultraviolet collector optics

Huatan Qiu, Shailendra N. Srivastava,* Keith C. Thompson, Martin J. Neumann, and David N. Ruzic

Center for Plasma Material Interactions, University of Illinois at Urbana-Champaign, 104 South Wright Street, Urbana, Illinois 61801, USA

*Corresponding author: sns@uiuc.edu

Received 11 October 2007; revised 19 January 2008; accepted 6 March 2008; posted 6 March 2008 (Doc. ID 88492); published 28 April 2008

Successful implementation of extreme ultraviolet (EUV) lithography depends on research and progress toward minimizing collector optics degradation from intense plasma erosion and debris deposition. Thus studying the surface degradation process and implementing innovative methods, which could enhance the surface chemistry causing the mirrors to suffer less damage, is crucial for this technology development. A Mo–Au Gibbsian segregation (GS) alloy is deposited on Si using a dc dual-magnetron cosputtering system and the damage is investigated as a result of time dependent exposure in an EUV source. A thin Au segregating layer is maintained through segregation during exposure, even though overall erosion in the Mo–Au sample is taking place in the bulk. The reflective material, Mo, underneath the segregating layer is protected by this sacrificial layer, which is lost due to preferential sputtering. In addition to theoretical work, experimental results are presented on the effectiveness of the GS alloys to be used as potential EUV collector optics material.

OCIS codes: 160.4670, 040.7480.

1. Introduction

Current lithography uses 193 nm light and can be extended down to the 45 and even 32 nm nodes through various resolution enhancement techniques. Beyond that, however, next generation lithography (NGL) methods are needed to meet the advancing expectations of Moore's law. The leading candidates for NGL are extreme ultraviolet (EUV) sources producing light at 13.5 nm [1–5].

The fuel ions (Xe or Sn) in discharge produced plasma (DPP) or laser produced plasma (LPP) EUV sources produce extremely high charge states on the order of +10 [6,7]. Both sources also produce strong electric fields during plasma expansion that can accelerate these ions to high energies on the order of 10 keV. The collector optics mirror surface will be bombarded by this potentially high flux of energetic ions, eventually damaging the surface and destroying the reflective properties of the mirror. The mechanisms for mirror degradation are surface erosion, roughening, deposition or implantation of impurities, and layer mixing. The Xtreme Commercial EUV Emission Device (XCEED) at the University of Illinois [8,9] has been developed to test the performance of various EUV mirror materials during operation of a commercial-scale EUV source and to investigate the mechanisms behind any observed losses in reflectivity.

An innovative idea using the Gibbsian segregation (GS) concept as the potential grazing incident EUV collector optics is developed and explored [10–13]. GS processes have been defined [14,15] as the tendency of certain solute elements in a homogenously interspersed solid solution to accumulate at imperfections, such as grain boundaries and interfaces in the bulk lattice that then may segregate to the free sur-

0003-6935/08/132443-09$15.00/0

faces. Since GS processes and phenomena occur at the surface, there is the potential for functional surface engineering to achieve the desired physical, chemical, electrical, and optical effects. The application of GS as the EUV collector optics in grazing incidence mirrors would require engineering of the surface for erosion resistance and self-healing characteristics while maintaining good surface smoothness and high-reflectivity over a longer period of time.

The energy deposition from the EUV and out-of-band light, together with the bombardments by the energetic ion debris, provide the potential driving forces for GS processes at the surface. For example, in a Mo–Au GS alloy, the segregation of Au (solute) will replenish the mirror surface from the bulk material of the GS alloy, so that the surface segregating Au layer serves as a sacrificial sputtering layer and leaves the Mo underneath virtually "untouched." If the regenerative transport processes (bulk, grain, interface diffusion) and surface renormalization are faster than the erosion time scale (i.e., the average time between large energy sputtering events), then the collector optics would be self-repairing. Early works have been published to assess the suitability of the GS alloy technology for early adoption of EUV lithography and test the validity with the theoretical estimate [10–13]. This work describes further experimental efforts to discover if GS alloys effectively ameliorate and self-heal the damage in grazing incidence EUV collector optics.

2. Experiment

High quality Mo–Au GS alloys are fabricated by a dual-magnetron cosputtering system (DMCS) at the Center for Plasma Material Interactions (CPMI). The fabricated Mo–Au GS samples are exposed in a Xe fueled DPP EUV source and the erosion, roughness, and composition are measured using scanning electron microscope (SEM), atomic force microscopy (AFM), and Augur electron spectroscopy (AES). In addition, *in situ* reflectivity is also measured on these samples.

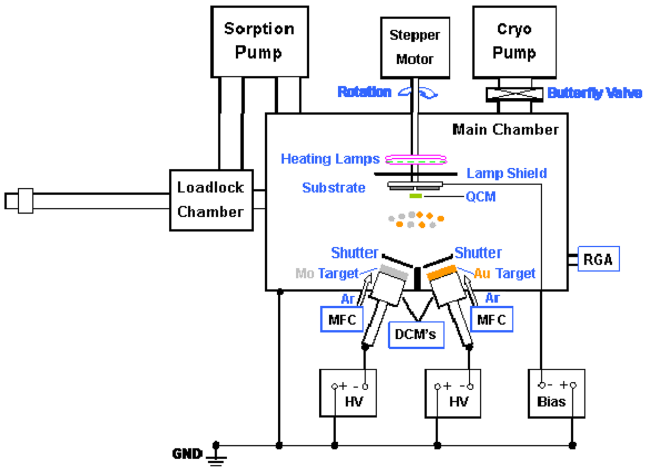

Fig. 1. (Color online) Dual-magnetron cosputtering system (DMCS) operating with two dc magnetron guns (2 in. diameter) at CPMI of UIUC.

A. DMCS Fabrication System

The Mo–Au GS alloys are produced by the DMCS system, as shown in Fig. 1, which is able to fabricate multiple thin film depositions (up to two simultaneous materials) and alloys on a heated substrate holder. Several features of the DMCS system are designed and achieved to fabricate the high quality Mo–Au GS films. The base pressure of the deposition chamber is maintained at an ultra high vacuum (UHV) of $\sim 4 \times 10^{-9}$ Torr to keep a clean and oxygen-free environment for the deposition processes. The substrate, together with the samples on it, is designed to be heatable, biasable, and rotatable. All possible sources of oxygen or air are minimized throughout the entire fabrication period. The experimental parameters, e.g., temperature and sample bias, are carefully determined based on the quality requirements.

Since there are two targets (Mo at 99.95% purity and Au at 99.99% purity) working together, the sputtered atoms will prefer to diffuse toward the substrate at a certain solid angle with respect to their own target location. Therefore, it is absolutely necessary to make the substrate (with four samples on it) rotatable so that both Mo and Au contents will reach the sample surfaces uniformly. This is achieved by a programmed stepping motor. Additionally, ultra high purity (UHP) Ar is used as the operation gas and is controlled by mass flow controllers. The Mo and Au targets are precleaned at high-power levels for at least 15 min presputtering with closed shutters to remove the surface oxide and contamination layer prior to the fabrication. To inhibit the formation of the native surface oxide layer, a capping layer of ~ 3 nm of Au is created to protect the Mo–Au alloy film against oxidation in all runs [16–18]. This also provides a higher initial surface enrichment of Au. In actual use as a collector mirror, this capping layer would be quickly eroded to a thickness on the order of a few atomic layers (~ 0.5 nm) and activate the segregation process. The Mo–Au GS alloys are fabricated using a recipe of 165 °C, 2 mTorr of UHP Ar, −100 V dc bias, 65 W dc power for the Mo target, and 1.7 W dc power for the Au target. The alloy ratio of Au is controlled in the range of 1–2% to avoid a significant reflectivity loss of the Mo film to the EUV light. The rms surface roughness is maintained at 1 nm or less to fit the requirement as a mirror film of the EUV collector optics. This roughness measurement is in the high spatial frequency range (HSFR) (nanometer range). It is surface roughness in the HSFR that leads primarily to a reduced reflectance.

B. Sample Exposure System

An XTREME Commercial Xtreme Technology Source (XTS) 13–35 nm DPP EUV source is fitted to a special diagnostics chamber called XTREME Commercial EUV Emission Device (XCEED) [8,9] as shown in Fig. 2. This allows mirror samples to be exposed to

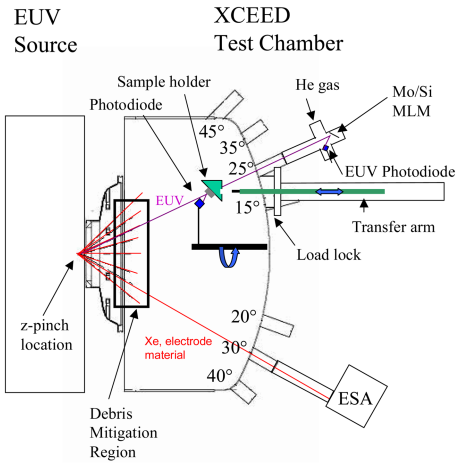

Fig. 2. (Color online) Schematic of the XCEED exposure tool at CPMI of UIUC.

a z-pinch Xe plasma. This plasma source uses Xe gas to create 35 W of EUV light (2% bandwidth) in 2π sr with a conversion efficiency (CE) of 0.55%. The source is configured to be operated at continuous pulse rates of 500 Hz with 2 mTorr Xe feeding gas. The mirror samples are exposed to millions of shots, and then carefully examined to determine the level of damage done to the mirror. The XCEED exposure tool is designed to characterize the EUV source plasma and the debris fields emitted by the DPP, along with optic samples exposed to the pinch plasma. The energy sector analyzer (ESA) [8,9] diagnoses ion debris emitted from the plasma source by energy-to-charge ratio using ion time-of-flight (ITOF) analysis. There are four sample locations in the XCEED chamber and it is equipped with a load-lock extraction port, Fig. 3. The load-lock system allows samples to be unloaded out of the chamber during tests at varying exposure durations without disturbing the EUV source operation and the remaining samples. This is critical to minimize transient effects that are caused by electrode thermal cycling from discontinuous source operation. A single load-lock system can be moved among the four sample positions to unload samples for analysis during testing. The sample holders are custom designed aluminum blocks with indentations for mirror sample positioning. Samples are attached to the sample holders with carbon tape and positioned to present the samples to the light source at either a 20° grazing or 80° normal incidence angle. In the present experiment, all samples are investigated at a 20° grazing incidence angle.

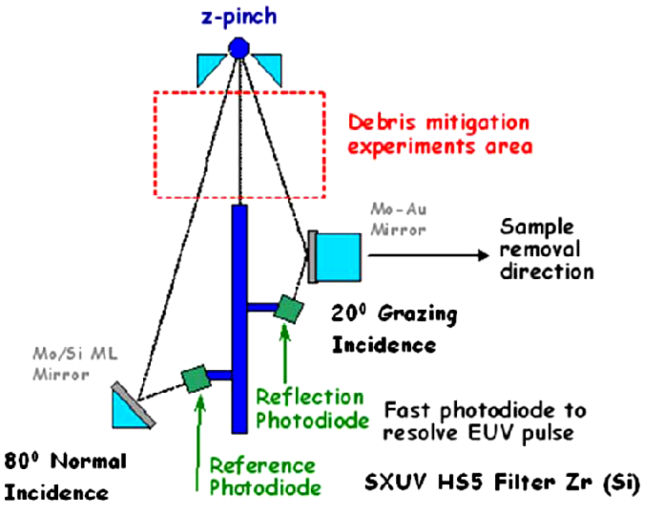

Fig. 3. (Color online) Schematic of the *in situ* reflectivity measurement in the XCEED system at CPMI of UIUC.

C. *In situ* Reflectivity Measurement

The exposed samples are placed at a distance of 56 cm from the pinch at a 20° grazing (70° to the normal) incidence angle. EUV directly from the source (reference) and reflected by the samples (reflection) is measured using two international radiation detectors (IRD) [19] SXUV HS5 Zr/Si EUV photodiodes. This type of photodiode is selected for the fast response in order to resolve the EUV lights from pinch pulses. The wavelength selectivity is available by a built-in Zr/Si filter limiting the response to wavelength less than 20 nm. The reference photodiode (88.7 cm from pinch) is mounted external to the chamber, but in vacuum on an angled port in a single bounce configuration using a specialized Mo/Si multilayer mirror that provides in-band selectivity for EUV light measurements. The multilayer with 50-pair Mo/Si bilayers is placed in the path of the reference EUV light at 10° normal incidence, which reflects the EUV lights to the reference photodiode (4.2 cm from the multilayer). This is to protect the reference photodiode against the direct bombardment by the energetic ion debris during the exposures. Additionally, there is a 2 mm orifice limiting particle flux and the assembly is back-filled with helium gas to mitigate damage to the multilayer mirror. The reflected EUV light by the mirror samples mounted in the chamber are detected by a reflection photodiode, which is placed 3.2 cm from the leading edge of the sample. The reflection photodiode with a shielding cap is affixed to the shaft of a motorized rotary feedthrough, and can be rotated to measure the reflected EUV lights from any of the four sample locations in the chamber.

Both the reference photodiode and reflection photodiode are shielded from direct debris impact, but are still subject to damage from reflected particles in the chamber. Note the difference in the EUV selectivity between the reference mirror and the reflection mirror: the reference signal comes from a 50-period multilayer mirror, whose narrow bandwidth dominates on the spectral selectivity of the photodiode; while the reflection signal coming from the 20° grazing incidence samples has a wider high-reflectivity bandwidth, which is reduced only when coupled to the photodiode (<20 nm wavelength selectivity) with a spectral range comparable to the reference one. The resulting bandwidth is approximately 4%.

Typically, the response of the photodiode to the EUV light emitted during a single pinch is a narrow

Table 1. SEM Results of the Time Duration Exposure Experiment[a]

Sample	Pre-Mo–Au	Post-#1	Post-#2	Post-#3	Pre-Ru	Post-Ru
Thickness [nm]	199.4	198.2	197.4	195.0	185.3	178.8
Erosion [nm]	—	1.2	2.0	4.4	—	6.5
No. of Shots	—	1.30 M	3.36 M	5.26 M	—	5.26 M

[a]Scalar error = 1 nm.

positive peak. The signal peak in each record point is the result averaged over 1024 continuous counts, and the integrable time interval is 5×10^{-10}s. Integrating the pulse area provides a value for the total energy of EUV light. *In situ* measurement results in damage to both the reflecting mirrors and the photodiode surfaces. Therefore, absolute reflectivity is not available. Practically, the obtained reflection signal will be offset by the background noise and integrated to get the integrated reflectivity in reflection. The integrated reflectivity in reference can be obtained by integrating the reference signal. A relative reflectivity is calculated through the division of the two integrated reflectivities. The relative reflectivity is normalized by their maximum, in order to eliminate the impact of the variation of the measure angle, the instability of the plasma pinch, and the other operational variations between different sample locations and different exposures. In this way, the individual *in situ* reflectivity measurements in different exposure runs can be qualitatively compared to each other in this normalized scale.

3. Results and Discussions

Three Mo–1.64% (±0.27%) Au GS samples, named as "Post-#1", "Post-#2", and "Post- #3", together with a commercial-level Ru sample (fabricated by Saša Bajt of Lawrence Livermore National Laboratory) for comparison, are exposed up to 5.26 million shots in a Xe fueled DPP EUV source at CPMI. A time dependent exposure test was performed, and the subsequent mirror surface damage was characterized. Based on the preinvestigations through the sudden variations in the reflectivity temporal signals, the samples are unloaded through a load-lock in the exposure chamber after 1.30 million, 3.36 million, and 5.26 million shots, respectively. Only Post-#3 is preheated to a temperature of 164 °C. Since Post-#3 does not have to be unloaded during the entire 5.26 million shots, a thermocouple can be mounted on it. The final temperature of this Mo–Au Post-#3 sample is 75 °C, the typical temperature after several millions of EUV shots in the XCEED system for any sample. The ion energy spectra and flux from the EUV plasma is measured by the ESA and the erosion is modeled based on the measured flux. The *in situ* reflectivity is measured at a 20° grazing incidence angle for all four samples. The evolution of the GS processes corresponding to the exposure scale, erosion, surface roughness change, self-healing mechanism, and reflectivity degradation was investigated in this time dependent exposure experiment. The reflectivity measured from the Ru sample is compared with the reflectivity from GS alloys.

A. Erosion

The best estimate of the thin film erosion is obtained by measuring the cross-sectional thickness of the pre- and postexposed samples by SEM for all four samples. It should be noted that the results are of limited accuracy for most of the small changes seen. As shown in Table 1, the erosions of the Mo–Au samples with exposure shots of 1.30 million, 3.36 million, and 5.26 million are 1.2 nm, 2.0 nm, and 4.4 nm, respectively. The Ru sample is eroded 6.5 nm after 5.26 million exposure shots, which is larger than the erosion of Mo–Au sample under the same exposure conditions. It should be noted that the error of the thickness measured from SEM picture is 1 nm due to the thickness of the scalar lines in cross-sectional pictures. Since the overall erosion in the Mo–Au sample took place in the bulk, it is important to look at AES results to verify if the segregation actually took place.

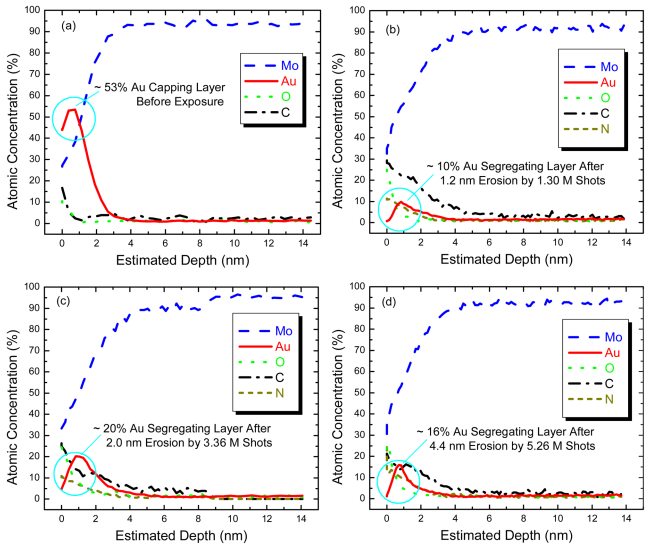

Fig. 4. (Color online) Depth profiles of the pre- and postexposed Mo–Au samples: (a) Preexposed Mo–Au sample with a ~3 nm Au capping layer, (b) postexposed Mo–Au sample after 1.30 million shots, (c) postexposed Mo–Au sample after 3.36 million shots, and (d) postexposed Mo–Au sample with a preheat temperature of 164 °C after 5.26 million shots.

B. Impurity Influence

Figure 4 shows the depth profiles of the pre- and post-exposed Mo–Au samples. Figure 4(a) shows a ~53 at.% Au on the preexposed Mo–Au sample. This high Au at.% partially comes from weak segregation at room temperature, but is mostly from the contribution of the thin Au capping layer. As seen in Figs. 4(b)–4(d), all three exposed Mo–Au samples show much higher Au at.% on the surface than the value in the bulk, which implies that the segregation is taking place since overall erosion in Mo–Au bulk was greater than the initial thickness of the capping layer. The Au at.% on the surfaces of the eroded Mo–Au samples is ~10, ~20, and ~16%, corresponding to 1.30 million, 3.36 million, and 5.26 million exposure shots, respectively.

In addition, three major impurities (O, N, and C) are found near the surface of all exposed Mo–Au samples, according to AES depth profile. An O peak always exists around 25 at.% at the top surface, but rapidly drops to "zero" within the top 1–2 nm depth. It is most likely caused by oxidation from exposing Mo–Au samples to air before AES analysis. A N peak usually exists around 10–20 at.% on the surface, and ranges up to 4 nm in depth. According to the intensity and penetration depth, N is more likely from the energetic ion implantation during the exposures from the nitride insulators of the source electrodes. A C peak is stronger (starting from ~20–30 at.% on the surface) and deeper (up to 6 nm in depth). It is likely due to redeposition during the exposure from the carbon tape attached at the back of the samples. The Mo depth profiles are almost the same compared to the preexposed and other exposed samples in the same exposure run. This implies that the Au in the original capping layer or segregating layer might be replaced with the impurities, such as N and C, in the near-surface depth. This replacement may decrease reflectivity.

Typically, the presence of C in the film surface will lower the overall sputtering yield. Potentially, it will affect the preferential sputtering of the Au segregating layer, and further weaken the GS performance. A theoretical investigation has been performed to study this impact. As shown in Fig. 5, the sputtering yield calculations using stopping and range of ions in matter (SRIM) [20] show that pure C has a similar yield as pure Mo when incident by Xe ions at a 20° grazing angle. Note that the Mo material in the Mo–Au alloy would be dramatically protected due to strong preferential sputtering of Au if a thin (say 0.5 nm) segregating layer could be maintained. Considering the penetration depth and the at.% of the C component obtained in the AES depth profile (Fig. 4), three film structures are constructed in order to examine the structure and/or composition change. All of them have a basic structure, including a 190 nm Mo–1%Au bulk layer, underneath a 10 nm Mo–15%Au–15%C layer near the surface film. However, one of them has a 0.5 nm ideal segregating Au layer, a second one has a 0.5 nm mixed segregating Au-C layer (i.e., 50%Au–50%C), while the last one has no segregating layer.

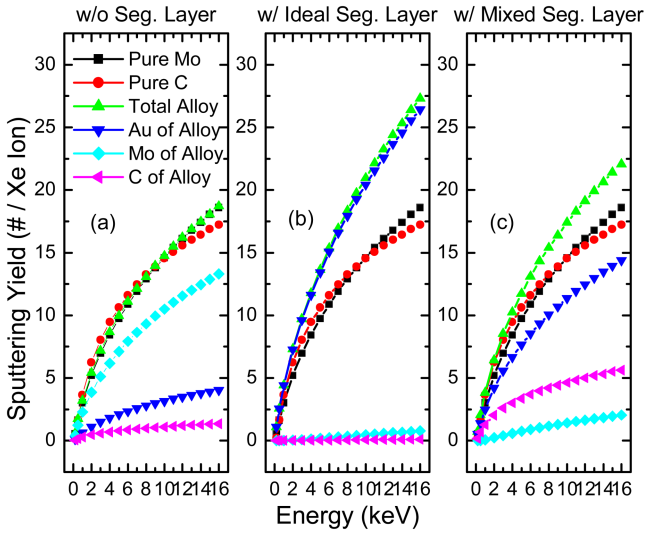

Fig. 5. (Color online) Sputtering yield calculations for impurity intermixed Mo–Au GS alloys.

According to Fig. 5(b), the Mo together with the implanted C could be protected due to the preferential sputtering of Au if an ideal segregating layer is still present. But, if there is no segregating layer as seen in Fig. 5(a), the Au in the intermixed near-surface (Mo, Au, and C) would lose the ability of preferential sputtering, and a significant loss of Mo would occur; however, this is not evident in SEM measurements. In the assumption that 50%Au was replaced with C in the 0.5 nm mixed segregating layer, Fig. 5(c) shows that the presence of C in the segregating layer still shows the preferential sputtering of Au but lowers its sputtering yield by up to 43% at 16 keV. The Mo would still be protected from the preferential sputtering of Au and partially from C, if the mixed segregating Au–C layer could be maintained all the time. Comparing the SEM erosion measurements, the case with a mixed segregating Au-C layer is more analogous to the real situation. In summary, the presence of C in the segregating layer and near-surface would somewhat lower the overall sputtering rate of segregated Au and enhance the sputtering of Mo. Thus, the GS efficiency would not be as high.

The N^+ is too light and fast to be resolved by the ESA device. But N^+ implantation will actually change the structure of the near-surface layers within a few angstroms to a few nanometers, further affecting the reflectivity of the mirror samples. This impact is discussed in detail later.

The above discussions indicate that the implantation of C and N components up to 6 nm in depth, is likely to change the segregating layer into a mixed structure, which is going to lower the GS performance. However, Au segregation and the preferential sputtering seem to still be taking place. To explain the GS behavior a simple three region model is proposed. Region I: in this region the Au capping layer is almost removed and the GS process is just initiated. Region II: in this region the GS process is fully activated and

Table 2. AFM Results for the Ru and Mo–Au Samples for the Time Duration Exposure Experiment[a]

Sample	Pre-Mo–Au	Post-#1	Post-#2	Post-#3	Pre-Ru	Post-Ru
Rms Roughness	0.86	0.63	0.89	0.61	0.34	0.90
Change (Post/Pre)	—	0.73×	1.03×	0.71×	—	2.67×
Maximum Height	7.05	12.19	8.80	7.51	2.40	9.48
No. of Shots	—	1.30 M	3.36 M	5.26 M	—	5.26 M

[a]Rms roughness and maximum height are in units of nanometers.

promoted to self-heal the eroded surface toward the new equilibrium between GS and erosion. Region III: in this region the GS process reaches its new equilibrium to dynamically balance the steady erosion to maintain the reflectivity at a new equilibrium level. The Post-#1 Mo–Au sample was unloaded after 1.30 million exposure shots with the lowest surface Au ~10 at.%, which is in the end of GS Region I. The Post-#2 Mo–Au sample was unloaded after 3.36 million exposure shots with the highest surface Au ~20 at.%, which is in GS Region II. The Post-#3 Mo–Au sample was unloaded after 5.26 million exposure shots with an intermediate surface Au ~16 at.%, which is in GS Region III. Therefore, the ~10, ~20, and ~16% surface Au seen in the order of 3 exposure scales correspond to the stages of Au capping removal, transition region, and GS equilibrium of the overall GS process, respectively.

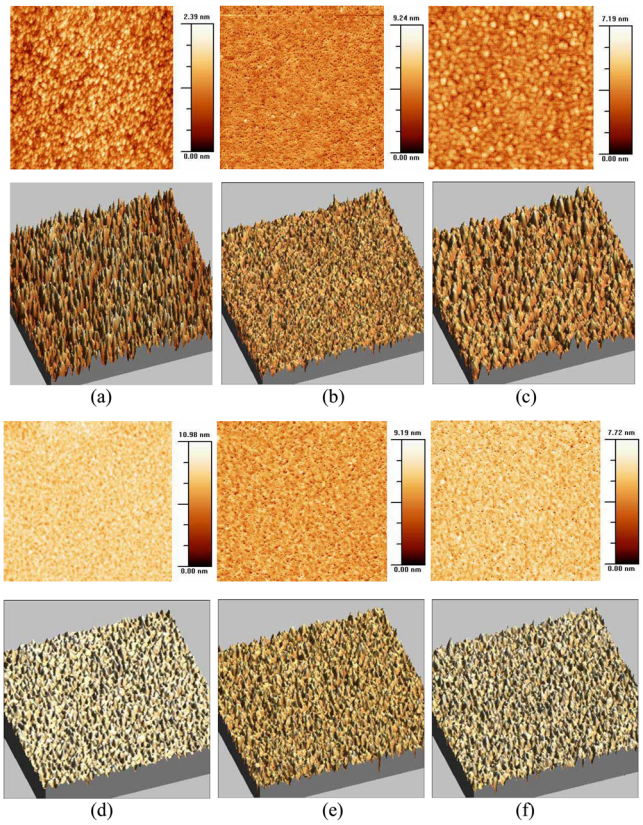

Fig. 6. (Color online) Rms roughness of the pre- and postexposed Ru and Mo–Au samples in 2D and 3D modes: (a) preexposed Ru sample, (b) postexposed Ru sample after 5.26 million shots, (c) preexposed Mo–Au sample with a ~3 nm Au capping layer, (d) postexposed Mo–Au sample after 1.30 million shots, (e) postexposed Mo–Au sample after 3.36 millionshots, and (f) postexposed Mo–Au sample with a preheat temperature of 164 °C after 5.26 million shots.

C. Surface Roughness

The rms surface roughness of the exposed samples is analyzed by AFM. As shown in Figs. 6(a)–6(f) and Table 2, the Ru sample after exposed to 5.26 million shots became much rougher (2.67×) than its preexposed value because of the erosions by the energetic ion debris during the EUV exposure, while the other three Mo–Au samples kept similar or smoother roughness (0.71 × –1.03×). It also implies that the Mo–Au GS alloy has a better erosion resistance than Ru. However, the changes in roughness and the height of the columnar islands of the surface of the exposed Mo–Au samples behave in a quite different way due to the effect of the GS. It can be explained by correlating the surface changes to the different stages of the GS process. According to

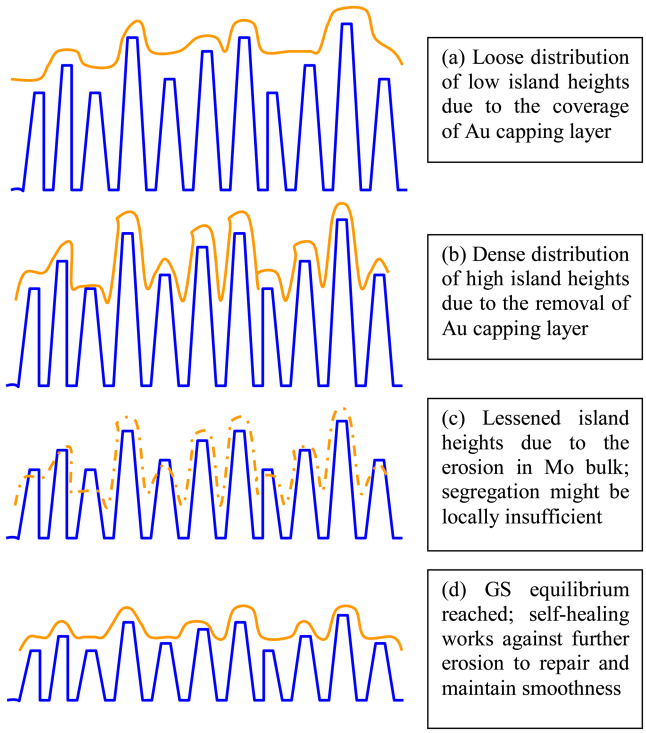

Fig. 7. (Color online) Graphical illustration of the profile heights of the columnar islands on the surface of the Mo–Au GS alloy (not in scale). Rigid profile represents the columnar islands of Mo–1% Au with a dense, tall microstructure. Overlaying profile represents the covered Au capping layer with a loose, low overall profile of surface height.

AFM results, the distribution of the height of the columnar islands on the film surface typically approximates normal distribution between zero and the maximum height of the columnar islands (H_{max}). Therefore, H_{max} can be considered as an indicator of the height of the overall islands on the film surface, i.e., the larger H_{max}, the higher the general columnar islands.

In the Au capping layer removal stage (Post-#1), the H_{max} increases (12.19 nm versus 7.05 nm) considerably, though the overall rms roughness became smoother (0.73×). The expression of rms roughness represents the standard deviation of the profile heights over a certain scan area. The preexposed Mo–Au sample has a loose distribution of the lower island heights ($H_{max} = 7.05$ nm) shown in Fig. 6(c), while the Post-#1 Mo–Au sample has a dense distribution of the higher island heights ($H_{max} = 12.19$ nm). Therefore, a higher overall island height and a lower rms roughness at the same time is seen in Au capping removal stage. As for the reason the island heights increase, it can be qualitatively interpreted by Fig. 7. The deposited Mo–1% Au bulk is characteristically dense and tall as described in Zone T of the Thornton diagram [21,22], represented by the rigid profile in Figs. 7(a) and 7(b). The Au capping layer produces the surface profile with a loose and low height distribution as represented by the overlaying profile in Fig. 7(a). In GS Region I, the Au capping layer is quickly eroded due to the strong preferential sputtering, so that the surface profile changes back to the dense, tall distribution as shown in Fig. 7(b). Thus there is an increase in H_{max}

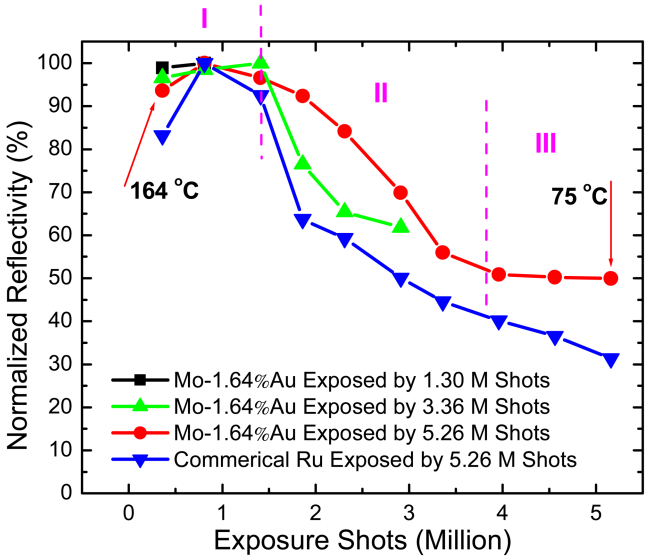

Fig. 8. (Color online) Normalized reflectivity measurements of the commercial Ru and the Mo-1.64%Au samples exposed to up to 5.26 million Xe EUV shots. Region I: in this region the Au capping layer is almost removed and the GS process is just initiated. Region II: in this region the GS process is fully activated and promoted to self-heal the eroded surface toward the new equilibrium between GS and erosion. Region III: in this region, the GS process reaches its new equilibrium to dynamically balance the steady erosion to maintain the reflectivity at a new equilibrium level.

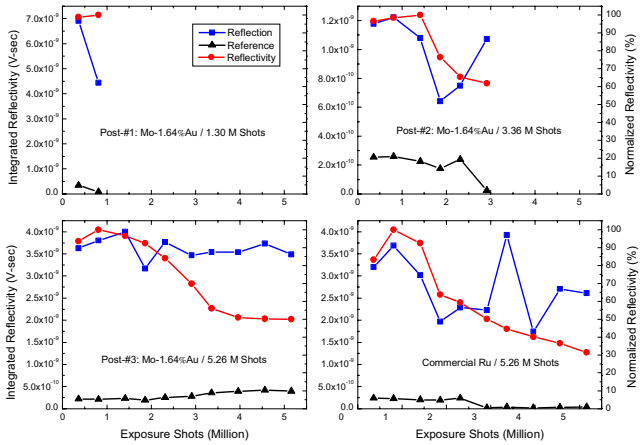

Fig. 9. (Color online) The integrated reflectivities of the reference and reflection signals of the exposed Ru and three Mo–Au samples. The unstable signals are from the impacts of the unstable EUV source emission, the degradation of the reflecting mirrors due from the ion erosion, the angular variations of the four measuring locations of the reflection photodiode, and the time difference of the measurements of the four samples at giving exposure time.

and a decrease in rms roughness seen at the same time.

In the GS transition stage (Post-#2), the H_{max} is lessened (8.80 nm versus 12.19 nm) while the rms roughness does not increase too much (1.03×), because the promoted GS process is trying to segregate more Au to self-heal the roughened surface as shown in Fig. 7(c). The erosion in Mo bulk takes place to lessen the high columnar islands. Because the erosion rates of the islands at different heights in particular for grazing incidence are different, the GS self-healing might be locally insufficient so that the islands' heights continue to be lessened. In the GS equilibrium stage (Post-#3), the surface roughness is smoothed to 0.71× of its preexposed value, and the H_{max} is repaired to be comparable to its original value (7.51 nm versus 7.05 nm), because the GS process achieved its new equilibrium between GS and steady erosion. As shown in Fig. 7(d), the segregating Au layer would sufficiently self-heal the steady erosive events by strong preferential sputtering and maintain the surface smoothness.

In summary, it is surmised that the continuous erosion produces high columnar islands on the surface leading to a rougher surface. On the other hand, ignoring the redeposition of C onto the film surface, the GS segregates Au onto the surface to effectively lessen the high columnar islands leading to a smoother surface. This seems to imply that the GS effect of self-healing works to repair and smooth the eroded surface.

D. Reflectivity

The normalized reflectivity is calculated as described in detail in Section 2.C and the results are shown in Fig. 8. For reference, we also show the integrated reflectivities of both reference and reflection signals of the four exposed samples in Fig. 9. The changes in the

normalized reflectivity of the exposed Ru and Mo–Au sample agree well with expectations about the GS stage classification. The three characteristic GS regions can be clearly seen in Fig. 8, which correspond to the three stages of the overall GS process. In GS Region I, represented by Post-#1 Mo–Au sample, the normalized reflectivity shows a little increase because the thin Au capping layer (~3 nm) is removed by the ion debris until a few monolayers are left. Then in GS Region II, represented by both the Post-#2 and Post-#3 Mo–Au samples after ~1.41 million shots, the normalized reflectivity decreases indicating the reflectivity degradation, because of the further erosion of the Mo bulk. In this region, the GS is fully activated to work against the reflectivity degradation by efficiently segregating more Au onto the eroded surface. Finally, in GS Region III, represented by Post-#3 Mo–Au sample, the normalized reflectivity is kept relatively flat but at a lower level when a new equilibrium between GS and steady erosion is achieved. This is also evidence of GS since the reflectivity does not continuously drop down to an unacceptably low level as is typical in the degradation of Ru and other EUV collector mirrors. The Post-#3 sample shows the full trend in reflectivity change as expected, which includes all typical characteristics in stages I–III of the whole GS process.

It is encouraging to see that all three exposed Mo–Au samples follow almost the same trend of the reflectivity change. The reflectivity of Post-#3 sample in degradation period keeps higher than the Post-#2 sample, because the former was preheated to a higher temperature of 164 °C while the latter was exposed at a much lower initial temperature without preheating. For comparison, the normalized reflectivity of the exposed Ru sample keeps dropping down to ~31.4% after 5.26 million exposure shots, while the exposed Mo–Au sample (Post-#3) is maintained at ~51.8% for the same exposure scale. This shows that the Mo–Au GS mirror can reach and maintain an equilibrium reflectivity level after a certain number of exposure shots, while the Ru mirror will continuously drop its reflectivity with increasing exposure shots. Moreover, this ~51.8% equilibrium reflectivity level results without any additional enhancement from the elevated temperature, which is a very effective driving force. Our separate works showed that the elevated temperature will additionally help the GS mirrors achieve even better reflectivity performance and less reflectivity degradation. The initial reflectivity of the Ru sample is relatively low, possibly because of the surface contamination, considering that this commercial-level Ru sample is originally smooth with only 0.34 nm rms roughness.

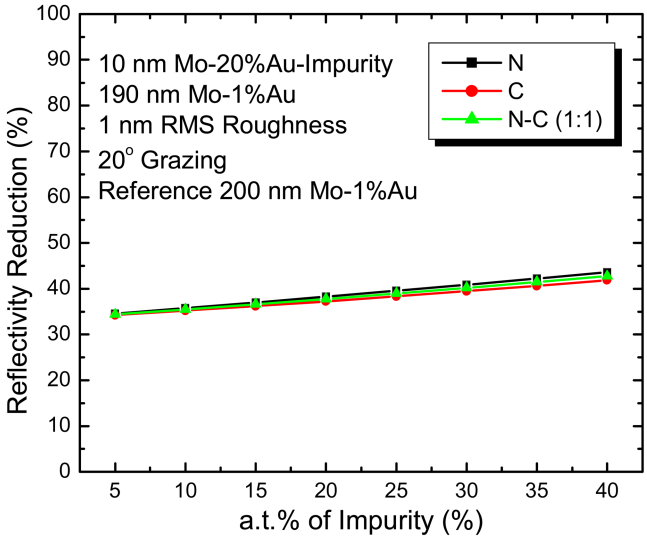

Fig. 10. (Color online) Theoretical estimate of the reflectivity reduction due to the presence of impurity in the first 10 nm of film of the Mo–1%Au GS alloy. The Au concentration in that 10 nm of film is fixed at 20% according to the AES depth profiles of the exposed Mo–Au samples. The Mo concentration in that 10 nm of film varies with the impurity components.

Note that the equilibrium reflectivity does not recover back to its maximum level even though both the roughness and the H_{max} are repaired to values that are comparable to its original values. This is because not only is the sample surface nonuniformly eroded, but also because the structure and concentration of Mo in the near-surface region (e.g., cascade region of energetic ion implantations up to tens of nanometers in depth) are modified by these implantations, redepositions, and cascade collisions. The theoretical reflectivity [23–25] was investigated, as shown in Fig. 10, involving N and C impurities on the surface together with the observed Au component (whether from the segregation or the original capping layer). Oxygen is not included since O is more likely from an external source. According to the AES depth profiles of the exposed Mo–Au samples, the test film is constructed to include a Mo–20%Au impurity layer in the first 10 nm of the film with the 190 nm Mo–1%Au bulk underneath. The Au concentration in that 10 nm film is fixed at 20% as commonly seen in the exposed Mo–Au samples, while the Mo at.% varies with the impurity components.

According to Fig. 10, the impurity presence of either N or C, or the combination of N–C (in 1 : 1 ratio) is likely to cause a large but similar reflectivity reduction. For example, assuming a N implanted GS Mo–Au film with 20%N and 20%Au presence in a depth of the top 10 nm followed by a 190 nm Mo–1%Au bulk, theoretical reflectivity is 42.3%, while the reflectivity of a 200 nm Mo–1%Au without N implantation under same conditions is 68.5%. This corresponds to a 38.2% reduction in normalized reflectivity, which is similar with the reduction measured in the equilibrium state (Fig. 8). More importantly, this agreement is repeatedly seen in the reflectivity measurements of the later experiments. Thus the reflectivity reduction in GS equilibrium is more likely because of the change of structure and composition in near-surface (say, 10 nm) region due to the implantation of N, redeposition of C, and/or other particles.

4. Conclusions

This study examined the effectiveness of the GS alloy as the grazing EUV collector mirrors. The experimental results suggest that Gibbsian segregation is operating in many aspects including self-healing the eroded surface, erosion resistance in the reflective optics, and reflectivity maintenance. The segregating Au from bulk of the Mo–Au alloy does work to effectively diffuse onto the surface, self-heal the damaged surface, resist the erosion of the reflective Mo, and reduce the reflectivity degradation. *In situ* reflectivity measurements imply that the normalized reflectivity could be maintained by effective GS process of self-healing and erosion resisting at elevated temperature. In addition it is observed that the implanted N and redeposited C, in the exposed Mo–Au GS alloys, affect the overall sputtering rate, replace Au to form a mixed segregating Au-C layer, and lower the GS efficiency correspondingly, as well as reduce the equilibrium reflectivity with respect to the maximum value.

We thank SEMATECH, Lawrence Livermore National Laboratory (LLNL), Sandia National Laboratory at Livermore (SNLL), Intel Components Research, and the Xtreme Technologies for support. A portion of this research was carried out in the Center for Microanalysis of Materials, University of Illinois, which is partially supported by the U.S. Department of Energy under grant DEFG02-91-ER45439. We also thank our undergraduate Jesse C. Anderson for the help with GS alloy fabrication and the buildup of DMCS system.

References

1. U. Stamm, "Extreme ultraviolet light sources for use in semiconductor lithography: state of the art and future development," J. Phys. D **37**, 3244–3253 (2004).
2. U. Stamm, I. Ahmad, V. M. Borisov, F. Flohrer, K. Gabel, S. Gotze, A. S. Ivanov, O. B. Khristoforov, D. Klopfel, P. Kohler, J. Kleinschmidt, V. Korobotchko, J. Ringling, G. Schriever, and A. Y. Vinokhodov, "High power EUV sources for lithography: a comparison of laser produced plasma and gas discharge produced plasma," Proc. SPIE **4688**, 122–133 (2002).
3. V. M. Borisov, A. V. Eltsov, A. S. Ivanov, Y. B. Kiryukhin, O. B. Khristoforov, V. A. Mishchenko, A. V. Prokofiev, A. Y. Vinokhodov, and V. A. Vodchits, "EUV sources using Xe and Sn discharge plasmas," J. Phys. D **37**, 3254–3265 (2004).
4. U. Stamm, J. Kleinschmidt, K. Gabel, H. Birner, I. Ahmad, D. Bolshukhin, T. D. Chinh, F. Flohrer, S. Gotze, G. Hergenhan, D. Klopfel, V. Korobotchko, B. Mader, R. Muller, J. Ringling, G. Schriever, and C. Ziener, "High power sources for EUV lithography: state of the art," Proc. SPIE **5448**, 722–736 (2004).
5. H. Kinoshita, "History of extreme ultraviolet lithography," J. Vac. Sci. Technol. B **23**, 2584–2588 (2005).
6. E. V. Lopez, B. E. Jurczyk, M. A. Jaworski, M. J. Neumann, and D. N. Ruzic, "Origins of debris and mitigation through a secondary RF plasma system for discharge-produced EUV sources," Microelectron. Eng. **77**, 95–102 (2005).
7. B. E. Jurczyk, E. V. Lopez, M. J. Neumann, and D. N. Ruzic, "Illinois debris-mitigation EUV applications laboratory," Microelectron. Eng. **77**, 103–109 (2005).
8. K. C. Thompson, E. L. Antonsen, M. R. Hendricks, B. E. Jurczyk, M. Williams, and D. N. Ruzic, "Experimental test chamber design for optics exposure testing and debris characterization of a xenon discharge produced plasma source for extreme ultraviolet lithography," Microelectron. Eng. **83**, 476–484 (2006).
9. E. L. Antonsen, K. C. Thompson, M. R. Hendricks, D. A. Alman, B. E. Jurczyk, and D. N. Ruzic, "Ion debris characterization from z-pinch extreme ultraviolet light source," J. Appl. Phys. **99**, 063301 (2006).
10. H. Qiu, K. C. Thompson, S. N. Srivastava, E. L. Antonsen, D. A. Alman, B. E. Jurczyk, and D. N. Ruzic, "Optical exposure characterization and comparisons for discharge produced plasma Sn extreme ultraviolet system," J. Micro/Nanolith. MEMS MOEMS **5**, 033007 (2006).
11. D. A. Alman, H. Qiu, T. Spila, K. C. Thompson, E. L. Antonsen, B. E. Jurczyk, and D. N. Ruzic, "Characterization of collector optic material samples exposed to a discharge-produced plasma extreme ultraviolet light source," J. Micro/Nanolith. MEMS MOEMS **6**,013006 (2007).
12. S. N. Srivastava, K. C. Thompson, E. L. Antonsen, H. Qiu, J. B. Spencer, D. Papke, and D. N. Ruzic, "Lifetime measurements on collector optics from Xe and Sn extreme ultraviolet sources," J. Appl. Phys. **102**, 023301 (2007).
13. H. Qiu, "Gibbsian segregation alloys driven by thermal and concentration gradients—a potential grazing collector optics used in EUV lithography," Ph.D. dissertation (University of Illinois at Urbana-Champaign, 2007).
14. P. A. Dowben and A. Miller, *Surface Segregation Phenomena* (CRC Press, 1990).
15. D. N. Ruzic, "Origin of debris in EUV sources and its mitigation," in *EUV Sources for Lithography*, Vivek Bakshi, ed. (SPIE Press, 2006), Chap. 36.
16. S. Bajt, H. N. Chapman, N. Nguyen, J. Alameda, J. C. Robinson, M. Malinowski, E. Gullikson, A. Aquila, C. Tarrio, and S. Grantham, "Design and performance of capping layers for extreme-ultraviolet multilayer mirrors," Appl. Opt. **42**, 5750–5758 (2003).
17. L. Gan, R. D. Gomez, C. J. Powell, R. D. Mcmichael, P. J. Chen, and W. F. Egelhoff, "Thin Al, Au, Cu, Ni, Fe, and Ta films as oxidation barriers for Co in air," J. Appl. Phys. **93**, 8731–8733 (2003).
18. S. Bajt, Z. R. Dai, E. J. Nelson, M. A. Wall, J. B. Alameda, N. Q. Nguyen, S. L. Baker, J. C. Robinson, and J. S. Taylor, "Oxidation resistance and microstructure of ruthenium-capped extreme ultraviolet lithography multilayers," J. Microlithogr. Microfab. Microsyst. **5**, 023004 (2006).
19. International Radiation Detectors Inc., Torrance, CA, www.ird-inc.com.
20. J. F. Ziegler, *The Stopping and Range of Ions in Solids* (Pergamon, 1985).
21. J. A. Thornton, "Influence of apparatus geometry and deposition conditions on the structure and topology of thick sputtered coatings," J. Vac. Sci. Technol. **11**, 666–670 (1974).
22. S. A. Campbell, *The Science and Engineering of Microelectronic Fabrication* (Oxford U. Press, 2001).
23. E. Gullikson, http://www-cxro.lbl.gov/optical_constants/.
24. B. L. Henke, E. M. Gullikson, and J. C. Davis, "X-ray interactions: photoabsorption, scattering, transmission, and reflection at $E = 50–30000\,\mathrm{eV}$, $Z = 1–92$," At. Data Nucl. Data Tables, **54**, 181–342 (1993).
25. B. L. Henke, P. Lee, T. J. Tanaka, R. L. Shimbukuro, and B. K. Fujikawa, "Low energy X-ray interaction coefficients: photoabsorption, scattering and reflection," At. Data Nucl. Data Tables **27**, 1–144 (1982).